PERGAMON

International Journal of Heat and Mass Transfer 42 (1999) 3307–3329

International Journal of HEAT and MASS TRANSFER

Mass diffusion-controlled bubbling and optimum schedule of thermal degradation of polymeric binders in molded powders

A.A.M. Oliveira [a], M. Kaviany [a,*], K.E. Hrdina [b], J.W. Halloran [b]

[a] *Department of Mechanical Engineering and Applied Mechanics, The University of Michigan, 2250 G.G. Brown, Ann Arbor, MI 48109-2125, USA*

[b] *Department of Materials Science and Engineering, The University of Michigan, 2250 GG Brown, Ann Arbor, MI 48109-2125, USA*

Received 14 April 1998; received in revised form 27 October 1998

Abstract

During the thermal removal of polymeric binders from molded powder specimens, the gas pressure of the species produced in the thermal degradation of the polymer may exceed the ambient pressure and then bubbling (a defect) occurs. Here the gas-pressure evolution in the early stages of thermal degradation is modeled using experimental degradation kinetics, thermodynamic models for the gas–liquid equilibrium, models for the diffusion coefficient, and the species conservation principle. The predicted results show a strong dependence of the instantaneous gas-pressure distribution within the specimen on the earlier temperature history and the initial concentration of the volatile product (pre-charge) formed during molding. Through simulations, the minimization of the processing time is addressed using successive constant (but different) heating-rate periods. It is shown that two distinct regimes exist, the pre-charge dominated and the generation-dominated regimes. A single-period heating-rate is dominated by the effect of the pre-charge which can cause bloating at low temperatures. A large number of periods allows for the progressive isolation of the effect of the pre-charge. It is shown that compared to the single-period, the processing time can be reduced by over 60% when a large number of varying heating-rate periods are used. Experiments are performed using poly[ethylene-*co*-(vinyl acetate)] (EVA) and silicon carbide particles, the results are compared with the predictions, and a good agreement is found.

1. Introduction

Binder removal is one stage in the manufacturing of near-net shape ceramic parts from ceramic powders. Polymeric binders (and additives) are added to the ceramic powders to enhance the flow characteristics of the dry powders thus allowing for molding into arbitrarily shaped parts (injection molding). Before sintering, the binder must be removed and thermal degradation is one of the methods used.

The removal of binders from ceramic bodies by thermal degradation can be described using poly[ethylene-*co*-(vinyl acetate)] (EVA) (a commonly used binder) as an example [1]. EVA suffers an early elimination reaction in which acetic acid is formed. Fig. 1 shows the degradation reaction of EVA in which acetic acid and poly[ethylene-*co*-(acetylene)] (PEA) are formed. If the diffusion coefficient of the degradation products through the polymer is sufficiently high, the

* Corresponding author. Tel: +1-734-936-0402; fax: +1-734-647-3170.

E-mail address: kaviany@umich.edu (M. Kaviany)

0017-9310/99/$ - see front matter
PII: S0017-9310(98)00363-9

Nomenclature

a_i	activity of species i
A_0	degradation-kinetics pre-exponential factor [1 s^{-1}]
$D_{A,l}$	binary diffusivity of species A [m^2 s^{-1}]
D_e	effective diffusivity of species A [m^2 s^{-1}]
D_0	diffusion pre-exponential factor (m^2 s)
h	specific enthalpy [J kg]
k_ϕ	chemical equilibrium constant [1 s^{-1}]
L	specimen thickness [m]
m	mass [kg]
$\dot{m}_A$	mass flux of species A at the surface [kg m^2 s^{-1}]
M	molecular weight [kg kmol]
n	order of the degradation reaction
$\dot{n}_d$	volumetric degradation rate [kg m^3 s^{-1}]
$\dot{n}_g$	volumetric generation rate [kg m^3 s^{-1}]
p	pressure [Pa]
R_g	universal gas constant [8314 J kmol K^{-1}]
t	time [s]
T	temperature [K]
u	specific internal energy [J kg^{-1}]
V	molar volume [m^3]
x	axial coordinate [m]
X	mole fraction
Y	mass fraction
Y_{A-PA}	mass of species A per kg of species PA
Y_{PA-T}	mass of species PA per kg of specimen.

Greek symbols

γ	activity coefficient
δ	solubility parameter [$MPa^{1/2}$]
ΔE_a	thermal degradation activation energy [J $kmol^{-1}$]
ΔE_d	diffusion activation energy [J $kmol^{-1}$]
ϵ	porosity
η	fraction of binder removed
ν	number of moles [kmol]
ρ	density, mass concentration [kg m^{-3}]
ϕ	volume fraction
χ	polymer–solvent interaction parameter.

Subscripts

a	ambient
A	acetic acid
e	effective
g	gas phase
H	enthalpy
i	species i, initial
l	liquid-phase
o	saturation, at $x=0$
P	poly[ethylene-*co*-(acetylene)] (PEA)
PA	poly[ethylene-*co*-(vinyl acetate)] (EVA)
s	solid phase, specimen
S	entropy
t	threshold

T	total
v	vapor phase
1	referring to a specific elapsed time
2	related to the state of minimum porosity of the specimen.

Other symbols

$\langle\ \rangle$	local volume-averaged
$\langle\ \rangle^i$	local phase-volume averaged.

products diffuse to the surface of the specimen where they are removed by evaporation. This is characterized by a reduction in the binder content $1-\eta$, as shown in Fig. 2(b), and by a reduction in the specimen thickness, as shown in Fig. 2(a). At the end of the period of formation and removal of acetic acid (elapsed time t_A), the PEA begins to degrade into smaller chains by a process of random chain scission. The products evolved also diffuse towards the surface and are evaporated. This causes a further reduction in the polymer volume, thus bringing the particles in the polymer matrix closer together. This process of shrinkage due to the polymer loss continues until the particles touch each other at an elapsed time t_2. The amount of EVA present at this stage is approximately 35% of the initial condition. After t_2 [Fig. 2(a)], further evaporation and removal of the polymer causes the formation of porosity. Finally at an elapsed time t_{A+P}, all the binder has been removed (the binder burnout is complete).

In the EVA system, the removal of acetic acid is a critical step, due to its relatively high volatility (boiling point of 118.2°C at pressure of 1 atm). If the diffusion rate is not sufficiently high, vapor nuclei are formed throughout the specimen as the temperature is raised. The surface of the particles may serve as the nucleation sites (heterogeneous nucleation). At high heating rates these vapor nuclei may become unstable and grow in the form of a bubble, thus forcing the ceramic particles apart. This is the bloating defect shown schematically in Fig. 3(a) and in the micrograph of Fig. 3(b) for an EVA–silicon carbide specimen.

Some of the existing theoretical models have focused on the early stages of the binder removal ($t < t_A$). These models assume that the amount of binder evaporated is not sufficient to cause the formation of open capillaries [2], or treat the formation of porosity assuming a prescribed distribution or calculating it using a shrinking-core model [3–5]. The models for the later stages of degradation, which are characterized by extensive porosity formation, address the capillary flow of the liquid binder [6,7].

One of the outcomes of the models has been the development of regime diagrams (binder removal maps). Shaw and Edirisinghe [5], extending the results of Evans et al. [2], have presented regime diagrams in

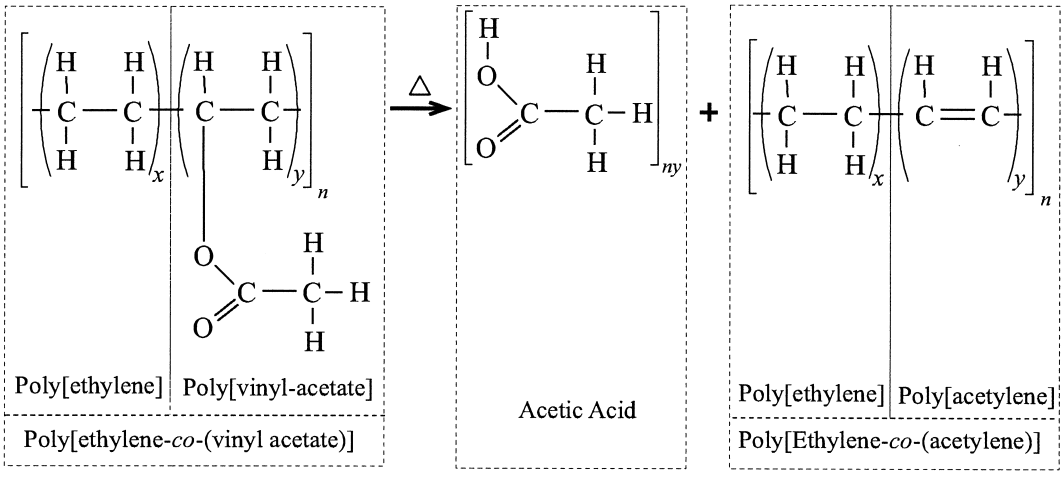

Fig. 1. Chemical formula for poly[ethylene-*co*-(vinyl acetate)] (EVA), poly[ethylene-*co*-(acetylene)], and acetic acid. Also represented is the elimination reaction producing acetic acid.

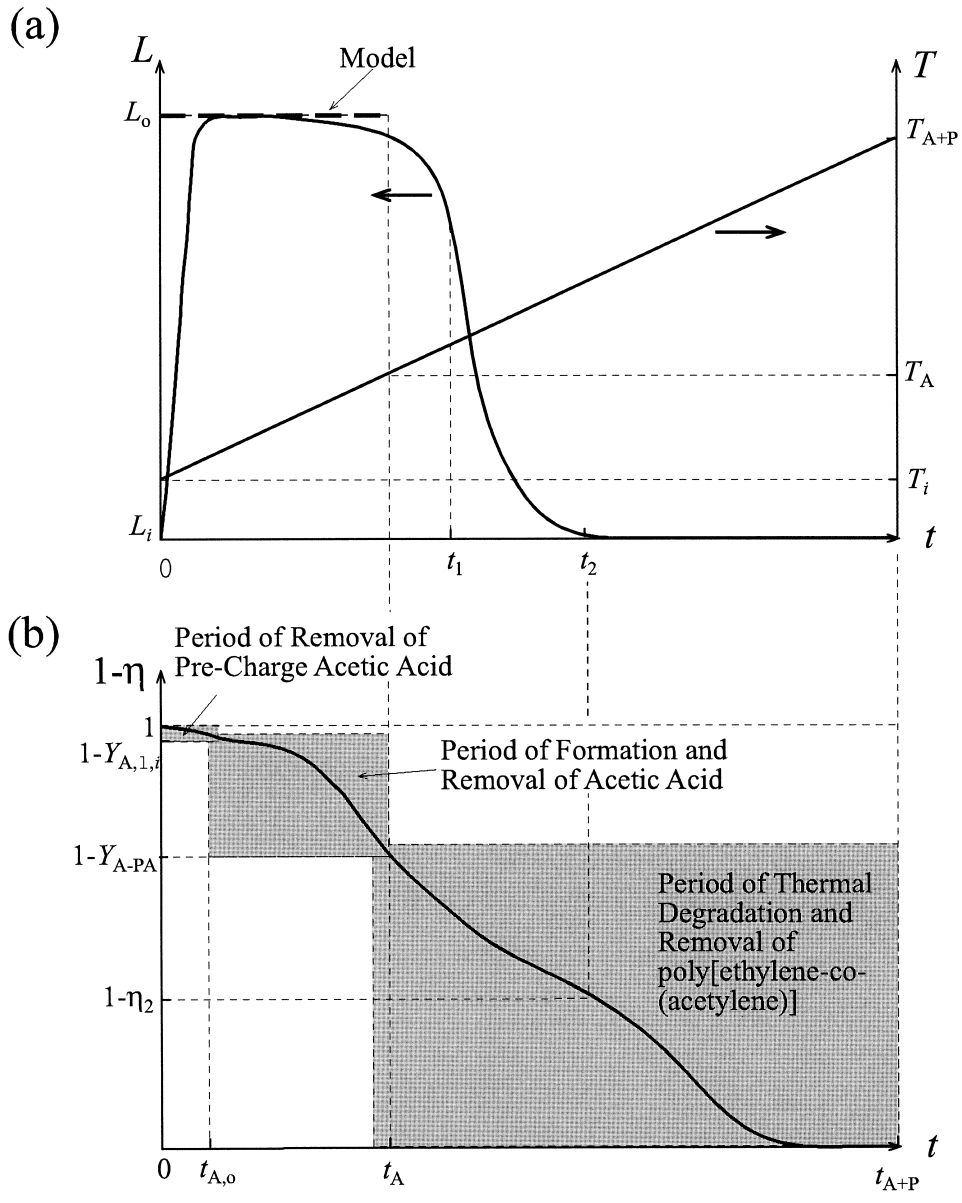

Fig. 2. Rendering of the variation of (a) the linear dimension of the specimen (e.g., thickness) L and temperature T, and (b) the fraction of binder remaining $1-\eta$, with respect to the elapsed time during thermal debinding at a constant heating rate.

which the critical heating rate (the heating rate for which the sample does not bloat) is mapped as a function of the sample thickness, the initial volume fraction of polymer, and the type of porosity formed. These regime diagrams can be used to select the heating rate for a single-period thermal debinding schedule, as the one shown in Fig. 2. Similar maps are obtained experimentally for EVA by Hrdina [1]. However, these maps do not readily provide an optimum multi-step heating schedule. A multi-step heating schedule has the advantage of reducing the total debinding time by adjusting the rate of temperature rise according to the rates of generation and diffusion. Pinwill et al. [8] has developed such a schedule experimentally. Their approach requires a large number of experiments and does not provide a complete understanding of the causes of bloating and of strategies to avoid bloating when the composition of the material is changed (e.g.,

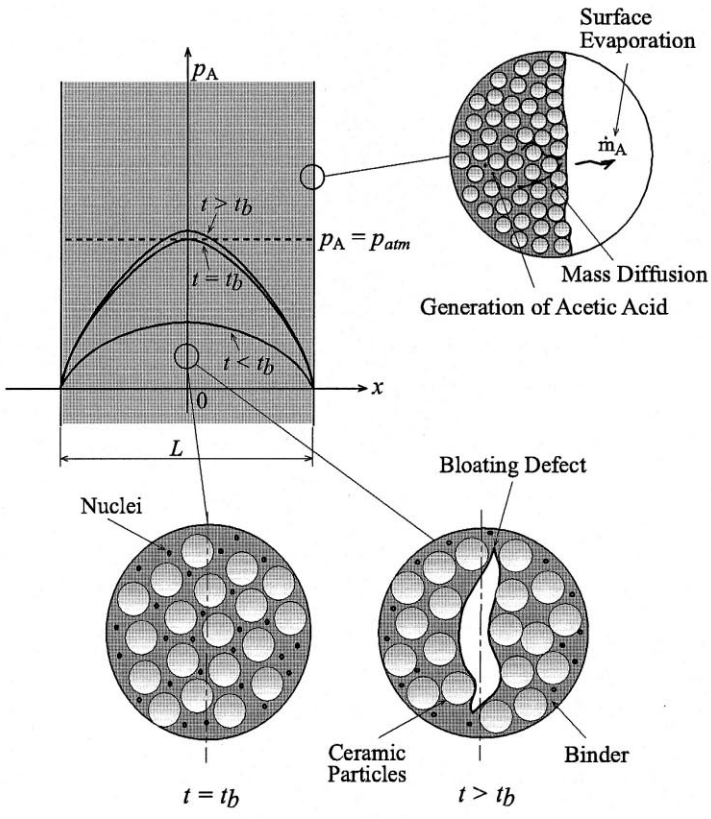

(a)

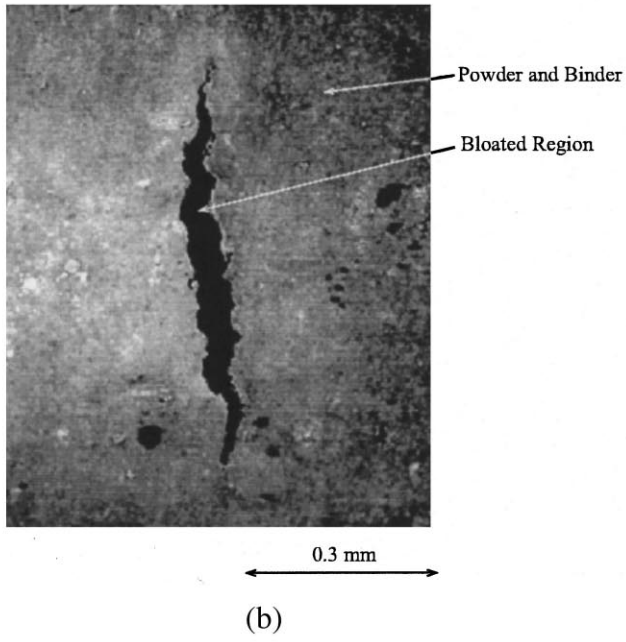

(b)

Fig. 3. (a) Rendering of distributions of the local partial pressure of acetic acid P_A during thermal debinding for a specimen with thickness L. The insets show the mass-diffusion paths, the onset of bloating (time t_b), and the bloating defect, which occurs for high heating rates. (b) Micrograph (SEM) of an EVA–silicon carbide (SiC) specimen showing the bloating defect.

low and high molecular weight component blends as a way of reducing viscosity while allowing for fast debinding [6,7]).

Here, the causes of bloating and the determination of an optimum schedule based on basic properties of the binder-ceramic system, for the early stages of thermal degradation (i.e., acetic acid elimination), are addressed. The gas pressure evolution is modeled using experimental degradation kinetics, the Flory–Huggins extension of the Scatchard–Hildebrand model for the gas–liquid equilibrium, an Arrhenius expression for the diffusion coefficient, and the species conservation principle. The particles are assumed stationary and the densities of the species are assumed constant. Zero mass transfer resistance is assumed at the specimen surface. The species conservation equation is solved numerically for concentration of acetic acid with prescribed heating rates and specimen sizes. The bloating is assumed to occur when the partial pressure of acetic acid in the centerplane of the specimen exceeds the threshold pressure, assumed equal to the ambient total pressure (the necessary superheating for bubble nucleation is assumed small and the effect of the normal stresses is neglected).

Experiments are performed using EVA and silicon carbide particles. EVA has been chosen here because of its commercial applications, its good molding properties, and, primarily, because of its well defined chemistry [12]. The side group elimination reaction, in which acetic acid is formed, occurs at temperatures smaller than those needed for the degradation of the PEA. Therefore, in this initial stage of degradation, the polymer yields a single, well-known product, which is completely eliminated before appreciable degradation of the remaining polymer chain (PEA) begins.

Another characteristic of this system is that an initial residual amount of acetic acid is generally present in the specimens due to thermal degradation during molding. This initial pre-charge can be responsible for the bloating occurring during short elapsed time for high heating rates when there is not sufficient time for the diffusion.

The development of the optimum schedule is based on the constraint that for a defect-free thermal debinding, the partial pressure of acetic acid should be smaller than (or equal to) the threshold pressure during the entire binder removal period. Then, for the minimization of the total debinding time, the maximum heating rate for each of a large number of heating periods of equal time increment is found. It is shown that this procedure leads to the minimum debinding time for a given binder system.

In the following, the analysis, the experiment, and the results are presented.

2. Analysis

The early elimination reaction of acetic-acid (here called species A) from the poly[ethylene-*co*-(vinyl acetate)] (whose repeating unit is called species PA) is modeled as a one-step chemical reaction. Thus, denoting the poly[ethylene-*co*-(acetylene)] repeating unit as species P, the early stage of thermal degradation of EVA can be represented, on a kmol of PA basis, as

$$\mathrm{PA} \rightarrow \nu_{\mathrm{A}}\mathrm{A} + \nu_{\mathrm{P}}\mathrm{P} \tag{1}$$

The mass of species A generated, per mass of species PA degraded, is a constant and it is denoted $Y_{\mathrm{A-PA}}$.

2.1. Species conservation equation

The species conservation equation is written in terms of volume-averaged quantities [13] and the local chemical and phase equilibria are assumed. The volume averaging of any quantity ψ is defined as

$$\langle\psi\rangle = \frac{1}{V}\int_V \psi \, \mathrm{d}V \tag{2}$$

where V is the volume of a representative elementary volume of all the phases.

The intrinsic volume-averaging of ψ for the phase β is the spatial averaging of that quantity over the volume occupied by the phase β only, i.e.,

$$\langle\psi\rangle^{\beta} = \frac{1}{V_\beta}\int_V \psi \, \mathrm{d}V \tag{3}$$

and $\langle\psi\rangle = \epsilon_\beta\langle\psi\rangle^{\beta}$, where ϵ_β is the volume fraction occupied by phase β.

Using the definitions above, a mass balance based on Eq. (1) gives

$$-\frac{\mathrm{d}\langle\rho_{\mathrm{PA,l}}\rangle}{\mathrm{d}t} = \frac{1}{Y_{\mathrm{A-PA}}}\frac{\mathrm{d}\langle\rho_{\mathrm{A,l}}\rangle}{\mathrm{d}t} = \frac{1}{Y_{\mathrm{P-PA}}}\frac{\mathrm{d}\langle\rho_{\mathrm{P,l}}\rangle}{\mathrm{d}t} = \langle\dot{n}_{\mathrm{d,PA}}\rangle \tag{4}$$

where $\langle\rho_{\mathrm{A,l}}\rangle$, $\langle\rho_{\mathrm{PA,l}}\rangle$, and $\langle\rho_{\mathrm{P,l}}\rangle$ are the local volume-averaged concentration of species A, PA, and P in the liquid phase and $\langle\dot{n}_{\mathrm{d,PA}}\rangle$ is the local volume-averaged homogeneous degradation rate of species PA, forming species A and P.

The conservation equations are applied to a planar geometry (Fig. 3), where the x-axis starts at the centerplane of the specimen. Assuming that species PA does not diffuse (i.e., it is stagnant), the conservation of species PA is given by

$$\frac{\partial\langle\rho_{\mathrm{PA,l}}\rangle}{\partial t} = -\langle\dot{n}_{\mathrm{d,PA}}\rangle. \tag{5}$$

The conservation of species A, assuming a dilute concentration (i.e., $\langle Y_{A,l}\rangle \to 0$), is given by

$$\frac{\partial \langle \rho_{A,l}\rangle}{\partial t} = \frac{\partial}{\partial x} D_e \frac{\partial \langle \rho_{A,l}\rangle}{\partial x} + \langle \dot{n}_{g,A}\rangle \tag{6}$$

where D_e is the effective mass diffusion coefficient of species A in the molded powder. The generation rate of acetic acid $\langle \dot{n}_{g,A}\rangle$ is

$$\langle \dot{n}_{g,A}\rangle = Y_{A-PA}\langle \dot{n}_{d,PA}\rangle. \tag{7}$$

The boundary and initial conditions are

$$x = 0, \quad \frac{\partial \langle \rho_{A,l}\rangle}{\partial x} = 0, \quad \frac{\partial \langle \rho_{PA,l}\rangle}{\partial x} = 0 \tag{8}$$

$$x = L/2, \quad \langle \rho_{A,l}\rangle = 0, \quad \frac{\partial \langle \rho_{PA,l}\rangle}{\partial x} = 0 \tag{9}$$

$$t = 0, \quad \langle \rho_{A,l}\rangle = \langle \rho_{A,l}\rangle_i, \quad \langle \rho_{PA,l}\rangle = \langle \rho_{PA,l}\rangle_i \tag{10}$$

where L is the specimen thickness and the initial ($t=0$) concentration of the species $A\langle \rho_{A,l}\rangle_i$ depends on the amount of pre-charge in the specimen and is assumed uniform.

The mass transfer coefficient at the specimen surface is assumed to be sufficiently large such that the surface concentration of acetic acid is equal to the free-stream concentration of acetic acid, which is equal to zero. The amount of initial pre-charge in the specimen is considered to be part of the total amount of acetic acid originally present in the EVA.

The time scale associated with the rate of change of the external temperature, for a heating rate of 20°C min^{-1}, is of the order of thousands of seconds. The diffusion time needed to reach a uniform temperature, assuming a unit Fourier number, for a 8 mm thick specimen is of the order of tenths of seconds. Also, the mass diffusivity for acetic acid in the specimen (as discussed below) is at least two orders of magnitude smaller than the thermal diffusivity. Therefore, the temperature along the specimen is assumed uniform and equal to the furnace temperature. The initial temperature is $T_i = 300$ K.

2.2. Thermal degradation kinetics

The thermal degradation of pure EVA has been studied before (e.g., [15,16]). During constant temperature decomposition, it is accepted that acetic acid is formed by a chain reaction. The initiation step is the thermal scission of the C—O bond in the PVA chain. A break of a C—O bond is accompanied by an abstraction of an H atom from an adjacent carbon to form acetic acid. This results in the formation of a double bond in the chain (i.e., formation of an acetylene group). The closest C—O bond to the double bond is weaker than the others and breaks in sequence originating a chain reaction (i.e., the propagation step). The rate of propagation increases as more chains are initiated. The steps in the dynamic decomposition [i.e., $T = T(t)$] seems to follow the same sequence. However, the mass loss as a function of temperature curves obtained from TGA experiments shift to higher temperatures as the heating rate dT/dt is increased and reach a limiting curve for very large heating rates. It has been shown by Hrdina [12] that the kinetics of EVA degradation for the filled system is different than the kinetics for pure EVA. Essentially, the thermal degradation in the filled system appears to start at lower temperatures when compared to the pure EVA. This has been explained as the result of the presence of an initial pre-charge of acetic acid formed during the specimen molding. Also, it is possible that the molding originates weak points along the chain which require a smaller activation energy to initiate the chain reaction, therefore, increasing the rate of initiation. Here, the kinetics of thermal degradation is treated empirically. Equations are developed and curve-fitted to the experimental thermal degradation rates.

The kinetics of the thermal degradation has been expressed (e.g., [2]) in terms of the fraction of binder removed η defined as

$$\eta = \frac{m_i - m}{m_i - m_f} \tag{11}$$

where m_i is the initial mass of the specimen, m_f is the final mass of the specimen (after the complete binder burnout), and m is the mass of the specimen at a given elapsed time.

Assuming a first-order, single-step reaction, the conservation of the binder (polymer and degradation products) species, for the removal during the acetic acid period, is written as

$$\frac{d\eta}{dt} = A_{o,\eta}(Y_{A-PA} - \eta)^n \exp\left(\frac{-\Delta E_a}{R_g T}\right) \tag{12}$$

where $Y_{A-PA} = 0.125$ for the EVA used, $A_{o,\eta}$ is the pre-exponential factor, n is related to the order of the reaction, ΔE_a is the activation energy, R_g is the universal gas constant, and T is the absolute temperature. Eq. (12) is valid for $\eta < 0.125$, which is equivalent to the early elimination reaction (i.e., elimination of acetic acid regime).

From Eq. (11), the fraction of binder removed can be related to the volume-averaged mass fraction of polymer $\langle Y_{PA,l}\rangle$ by

$$\eta = Y_{A-PA}\left(1 - \frac{\langle Y_{PA,l}\rangle}{Y_{PA-T}}\right) \tag{13}$$

where Y_{PA-T} is the mass of species PA per mass of specimen (here, $Y_{PA-T}=0.222$).

The volume-averaged mass fraction of PA is related to the mass concentration of PA by

$$\langle Y_{PA,l}\rangle = \frac{\langle \rho_{PA,l}\rangle}{\langle \rho\rangle} \tag{14}$$

where $\langle\rho\rangle$ is the total local volume-averaged density of the molded specimen.

From Eqs. (13) and (14), the degradation kinetics can be written as

$$\langle \dot{n}_{d,PA}\rangle = \langle\rho\rangle A_o(\langle Y_{PA,l}\rangle)^n = \exp\left(\frac{-\Delta E_a}{R_g T}\right) \tag{15}$$

where, A_o is the pre-exponential factor related to $A_{o,\eta}$ by

$$A_o = A_{o,\eta}\left(\frac{Y_{A-PA}}{Y_{PA-T}}\right)^{n-1}. \tag{16}$$

Note that the activation energy in Eq. (15) is the same as that in Eq. (12). Eq. (15) will be used in the remainder of this work.

The use of a single-step Arrhenius-type relation to model the dynamic decomposition, usually results in a heating-rate dependent pre-exponential factor and activation energy [15]. The isothermal decomposition is usually described as a one-step chemical reaction. In the limit of high heating rates the degradation kinetics may also exhibit an Arrhenius-type behavior. The dependence of the pre-exponential factor, activation energy, and reaction order on the heating rate will be taken into account later.

2.3. Diffusion coefficient

The effective mass-diffusion coefficient of species A in the molded powder is calculated from the Neale and Nader model [12] and is given by

$$D_e = D_{A,l}\frac{2\epsilon}{3-\epsilon} \tag{17}$$

where $D_{A,l}$ is the mass-diffusion coefficient of species A in the liquid phase (P + PA) and ϵ is the porosity of the molded compacts.

The mass-diffusion coefficient of species A in the liquid phase is assumed constant with concentration and is modeled with an Arrhenius-type dependence on temperature [14,17], i.e.,

$$D_{A,l} = D_o \exp\left(\frac{-\Delta E_d}{R_g T}\right) \tag{18}$$

where D_o is the diffusion pre-exponential factor and ΔE_d is the diffusion activation energy (constants).

The assumption of negligible dependence on the species concentration is justified by the relatively high degradation temperatures (much larger than the melting temperature of the polymer, $T_{ls}=80^\circ C$). Thermodynamic factors (i.e., nonideal effects on the chemical potential of the migrating species) are also negligible due to the expected dilute concentrations of acetic acid. Here, the parameters for the diffusivity of acetic acid in the polymer are obtained empirically from the TGA for specimens in which the mass loss is diffusion limited.

2.4. Thermodynamics

The partial pressure of A, p_A, in thermodynamic equilibrium with the liquid solution is,

$$p_A = p_o a_A \tag{19}$$

where p_o is the saturation pressure of species A at the temperature T and a_A is the activity of species A in the liquid solution.

From the Flory–Huggins theory, the activity coefficient of A in the liquid solution, γ_A, under the assumption that $V_A/V_{PA}\ll 1$, is [9–11]

$$\ln(\gamma_A) = (1-\phi_{A,l}) + \chi(1-\phi_{A,l})^2 \tag{20}$$

where $\phi_{A,l}$ is the volume fraction of species A in the liquid phase and γ_A is defined as $\gamma_A = a_A/\phi_{A,l}$ (i.e., the ideal solution limit is defined in terms of $\phi_{A,l}$).

The polymer–liquid interaction parameter χ can be expressed as a sum of an entropic contribution χ_S and an enthalpic contribution χ_H. The entropy part is assumed constant and equal to 0.34 and the enthalpy part is obtained from the Scatchard–Hildebrand model [9,10]. Then, the equation for χ becomes

$$\chi = 0.34 + \frac{V_A}{R_g T}(\delta_{PA}-\delta_A)^2 \tag{21}$$

where V_A is the molar volume of species A and δ_A and δ_{PA} are the solubility (Hildebrand or cohesion) parameters of species A and PA in the solution.

This relation neglects the dependence of χ on concentration, which occurs for some systems [11]. The solubility parameters are treated here as empirical constants and are determined from bloating experiments.

The volume fraction of species A in the liquid phase, assuming that $\rho_{P,l}=\rho_{PA,l}$ and using $Y_{A,l}=\langle\rho_{A,l}\rangle/\epsilon\langle\rho\rangle^1$ for the mass fraction of A in the liquid polymer, is related to the volume-averaged mass concentration of A through

$$\phi_{A,l} = \frac{\langle\rho_{A,l}\rangle\rho_{PA,l}}{\langle\rho_{A,l}\rangle\rho_{PA,l} + (\epsilon\langle\rho\rangle^1 - \langle\rho_{A,l}\rangle)\rho_{A,l}} \tag{22}$$

Table 1
Physicochemical properties of binder, its thermal degradation products, and powder

Component	M, kg kmol^{-1}	ρ, kg m^{-3}	V, m^3 kmol^{-1}	δ, MPa$^{1/2}$
Acetic acid (A)	60	1049.2	57.1×10^{-3}	21.3
EVA (PA)	114[a]	952	114×10^{-3a}	11.4
Poly[ethylene-*co*-(acetylene)] (P)	54[a]	952	54×10^{-3a}	11.4
SiC	40	3200	12.5×10^{-3}	–

[a] For the repeating unit.

where $\rho_{PA,l}$ is the density of species PA liquid, $\rho_{A,l}$ is the density of species A liquid, and $\langle\rho\rangle^l$ is the density of the liquid polymer (all the densities are assumed constant).

In the determination of the degradation kinetics, the fraction of binder removed η has been related to the volume-averaged mass fraction of PA by Eq. (13). However, more generally (for arbitrarily thick specimens) the fraction of binder removed observed in the TGA experiments is obtained from the mass balance at the surface of the specimen ($x=L/2$). For the elimination of acetic acid this gives

$$\eta=\frac{1}{\rho_{PA,l}\epsilon L/2}\int_0^t\langle\dot{m}_{A,l}\rangle\,dt \tag{23}$$

where the mass flux of A at the surface is

$$\langle\dot{m}_{A,l}\rangle=-D_e\frac{\partial\langle\rho_{A,l}\rangle}{\partial x}\bigg|_{x=L/2}. \tag{24}$$

Here, the TGA results will be presented in terms of the fraction of binder remaining, $1-\eta$.

3. Experiment

A detailed description of the experiments is given by Hrdina [1]. The polymer used here is known as ELVAX 470. The weight-averaged molecular weight (M_w) is 250,000 kg kmol^{-1}, the crystallinity is 6%, the glass transition temperature is -40°C, and the melting temperature is 84°C. The powder used is composed primarily of silicon carbide (α-SiC) with a small addition of aluminum oxide (Al_2O_3) and yttria (Y_2O_3). The average diameter of the particles is 0.5 μm. Table 1 presents the physicochemical properties of the ceramic, polymer and degradation products.

The specimen preparation consists basically in the preparation of the powder, shear mixing with the polymer at 90°C, and finally molding in a uniaxial die. During the shear mixing, due to the high shear caused by the introduction of the powder, there is an increase in temperature to 150–160°C. The stress caused by the shear mixing and the temperature above 150°C can be responsible for the existence of an initial pre-charge of acetic acid.

The molded specimens are then subjected to TGA and bloating tests.

3.1. TGA

Thermal Gravimetric Analysis (TGA) on small-size specimens is used to obtain the kinetics of the thermal degradation of the polymer. The specimens have an average mass of 25 mg, and precautions are taken to keep the cross-sectional dimensions under a millimeter in size. The specimens are placed on a platinum pan and heated in a flowing nitrogen environment at constant heating rates. The heating rates used are 0.1, 0.5, 1, 2, 4, 8, and 16°C min^{-1} [Fig. 4(a)]. In these small-size specimens, the diffusion lengths are small, therefore minimizing the influence of the internal mass diffusion in the mass loss observed during the TGA experiments. This has been verified by using small specimens with different sizes and obtaining the same mass loss curves. Also, experiments were performed at different nitrogen mass flow rates and the effect of the external mass transfer rates was found negligible. The mass loss can then be directly related to the kinetics of the thermal degradation (generation of acetic acid) through Eq. (15).

3.2. Bloating

The bloating temperatures are used to obtain the empirical solubility parameters δ_{PA} and δ_A for the acetic acid-polymer system.

For the measurement of the bloating temperature, a three-zone tube furnace is used. The specimens are placed in the furnace standing upright, and heated at different heating rates under a nitrogen atmosphere. The specimens are short cylindrical disks with diameter 25.4 mm and the thicknesses used are 0.5, 1, 2, 3, 4, 6, and 8 mm. After heating to the desired temperature, the specimens are cooled down to the ambient temperature and visually inspected for bloating.

Table 2
Properties for the specimens used in the calculations

$\langle\rho\rangle^1$, kg m^{-3}	952			
ϵ	0.49			
Y_{A-PA}	0.125			
Y_{PA-T}	0.222			
$\langle\rho\rangle$, kg m^{-3}	2098.48			
	Pre-charge			
$\langle\rho_{A,l}\rangle_i/\langle\rho\rangle$	0	0.0015	0.0021	0.0031
$\langle\rho_{A,l}\rangle_i$, kg m^{-3}	0	3.15	4.41	6.72
$\langle\rho_{PA,l}\rangle_i$, kg m^{-3}	466.48	441.28	431.23	412.76
$\langle\rho_{P,l}\rangle_i$, kg m^{-3}	0	22.05	30.87	47.01

4. Results and discussion

The conservation equations are solved numerically using an implicit finite-volume method. Initially, the empirical parameters for the model (parameters for the degradation kinetics, diffusion coefficient, and vapor–liquid equilibrium) are obtained using some experimental results. After these parameters are determined, the bloating temperatures predicted by the model are compared with the measurements and the effect of the pre-charge is discussed. Then, the optimum schedule is developed, beginning with a single-period schedule. Table 2 presents the properties for the specimens used in the calculations.

4.1. Experimental determination of kinetics, diffusion, and activity parameters

4.1.1. Kinetic parameters

The parameters necessary for the kinetics model were obtained through the application of empirical equations to independent TGA experiments. Eq. (15) [with Eq. (5)] is curve fitted to the rates of degradation determined experimentally. It has been shown by Hrdina [12] that the kinetics of thermal degradation does not follow a simple Arrhenius relation for the heating rates used. Here, in an attempt to best curve fit the experimental results, the kinetics of degradation for each heating rate is divided into a zeroth-order regime and a first-order regime. For each of these regimes, A_o and ΔE_a are obtained and curve fitted as functions of the heating rate dT/dt.

For A_o, we have

$$\ln\left[\frac{A_{o,\infty}-A_o}{A_{o,\infty}-A_{o,0}}\right]=-a_1\left(\frac{dT}{dt}\right)^{-a_2} \tag{25}$$

where the constants are $A_{o,\infty}=113.38$ s^{-1}, $A_{o,0}=0.03$ s^{-1}, $a_1=0.0201$, and $a_2=1.84$, for the zeroth-order regime, and $A_{o,\infty}=1.51\times10^8$ s^{-1}, $A_{o,0}=0$ s^{-1}, $a_1=0.000194$, and $a_2=2.90$, for the first-order regime.

For ΔE_a, we have

$$\ln\left[\frac{\Delta E_{a,\infty}-\Delta E_a}{\Delta E_{a,\infty}-\Delta E_{a,0}}\right]=-a_3\left(\frac{dT}{dt}\right)^{-a_4} \tag{26}$$

where the constants are $\Delta E_{a,\infty}=65.26$ kJ mol^{-1}, $\Delta E_{a,0}=41.51$ kJ mol^{-1}, $a_3=0.893$, and $a_4=0.722$, for the zeroth-order regime, and $\Delta E_{a,\infty}=161.4$ kJ mol^{-1}, $\Delta E_{a,0}=-63.5$ kJ mol^{-1}, $a_3=1.15$, and $a_4=0.142$, for the first-order regime.

The fraction of polymer remaining for which the degradation kinetics switches over from the zeroth-order regime to the first-order regime $\eta_{0\to1}$ is obtained from

$$\eta_{0\to1}=1-a_5\left(\frac{dT}{dt}\right)^{-a_6} \tag{27}$$

where the constants are $a_5=0.966$ and $a_6=0.0116$.

Using Eqs. (25) and (26), Eq. (15) becomes

$$\begin{aligned}\langle\dot{n}_{d,PA}\rangle=\langle\rho\rangle A_{o,0}(\langle Y_{PA,l}\rangle)^n\\ \times\exp\left(\frac{-\Delta E_{a,0}}{R_gT}\right)\left\{\left(\frac{A_{o,\infty}}{A_{o,0}}-\left(\frac{A_{o,\infty}}{A_{o,0}}-1\right)\right.\right.\\ \left.\times\exp\left[-a_1\left(\frac{dT}{dt}\right)^{-a_2}\right]\right)\\ \times\exp\left[-\left(\frac{\Delta E_{a,\infty}-\Delta E_{a,0}}{R_gT}\right)\right.\\ \left.\left.\times\left(1-\exp\left[-a_3\left(\frac{dT}{dt}\right)^{-a_4}\right]\right)\right]\right\}\end{aligned} \tag{28}$$

Therefore, the reaction rate is represented as a product of the kinetics of the isothermal degradation and a function that corrects for the dynamic degradation (between braces). Note that the limit for high heating rates reduces to a simple one-step reaction kinetics model.

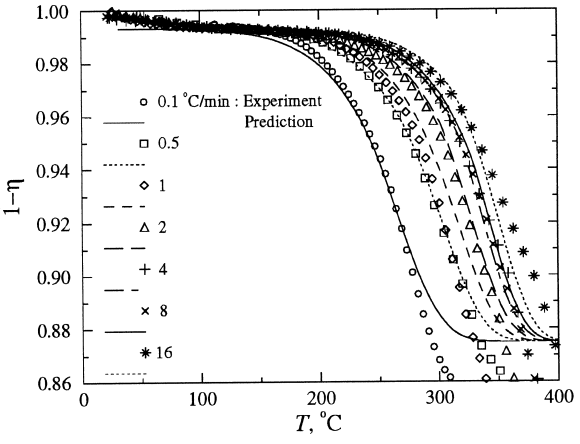

(a)

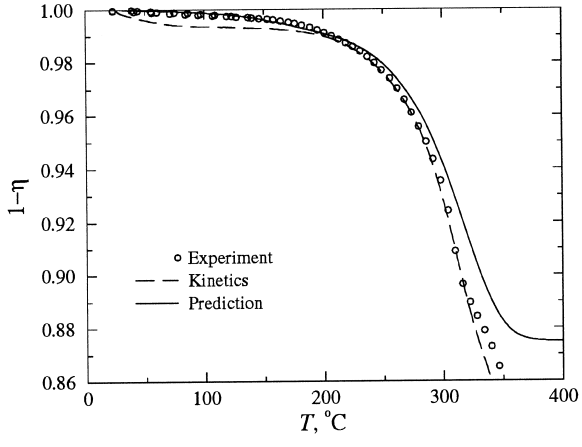

(b)

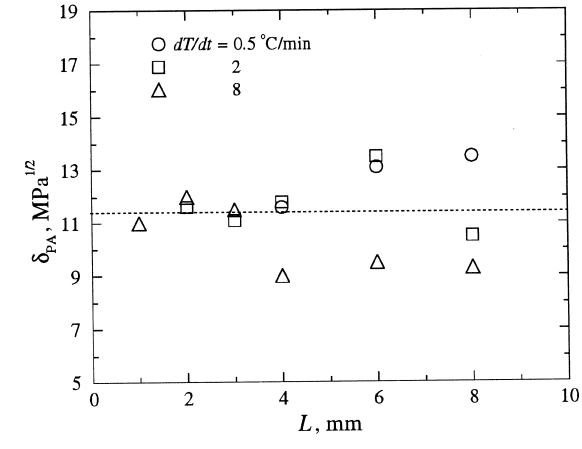

(c)

The constants in Eqs. (25)–(28) refer to dT/dt in °C min^{-1}. Fig. 4(a) shows the predicted and measured TGA curves for the heating rates used. The agreement for lower temperatures is generally good. The TGA curves present an initial weight loss for relatively low temperatures (for which thermal degradation of EVA is not expected to occur). These initial weight losses can be explained in terms of a pre-charge. The presence of a pre-charge has been cited by others [2]. This initial content of pre-charge is estimated from the TGA curves as being equal to $\langle\rho_A\rangle_i/\langle\rho\rangle = 0.0015$ (i.e., $\eta = 0.007$). The amount of volatiles adsorbed on the solid surface (e.g., water), as well as the equipment accuracy, accounted for, at most, only 10% of the amount of pre-charge recorded [12]. Therefore, all the initial weight loss (i.e., weight loss for temperatures below 150°C) was assumed to be due to the evaporation of the pre-charge. For larger temperatures, the period for the degradation of the PEA overlaps the acetic acid removal period, evidenced by the continual binder removal beyond $\eta = 0.125$. A treatment of polymer chain degradation can be found in Barone and Ulicny [6].

4.1.2. Diffusion parameters

A second TGA instrument has been used to measure the mass loss from a 2 mm thick specimen at a heating rate of 1°C min^{-1}. The conservation of mass equations, Eqs. (5) and (6), are solved, using the kinetics for $dT/dt = 1$°C min^{-1}, and the pre-exponential factor and activation energy for diffusion are chosen to match the measured and predicted TGA curves. The values obtained are $D_o = 2.5 \times 10^{-3}$ m^2 s^{-1} and $\Delta E_d = 55 \times 10^6$ J $kmol^{-1}$. Fig. 4(b) shows the measured and predicted results. Also shown are the measured and predicted results for the small specimen (the one used to obtain the parameters for the thermal degradation kinetics). The values obtained are able to curve fit the measured results for high binder content. The discrepancy between the predicted and the measured values may be due to a concentration dependency of the diffusion coefficient [14]. The effect of the variation of the porosity is expected to be negligible.

Fig. 4. (a) Measured and predicted binder removal history for very small samples using different constant heating rates (these data are used in determining the thermal-degradation kinetic parameters). (b) Measured and predicted binder removal for a 2 mm thick specimen heated at a constant heating rate of 1°C min^{-1}. Also shown is the measured binder removal for a very small sample at the same heating rate (kinetics). (c) Variation of the polymer solubility parameter δ_{PA}, determined from matching the predicted and measured bloating temperatures, as a function of the specimen thickness L. Results are for three heating rates.

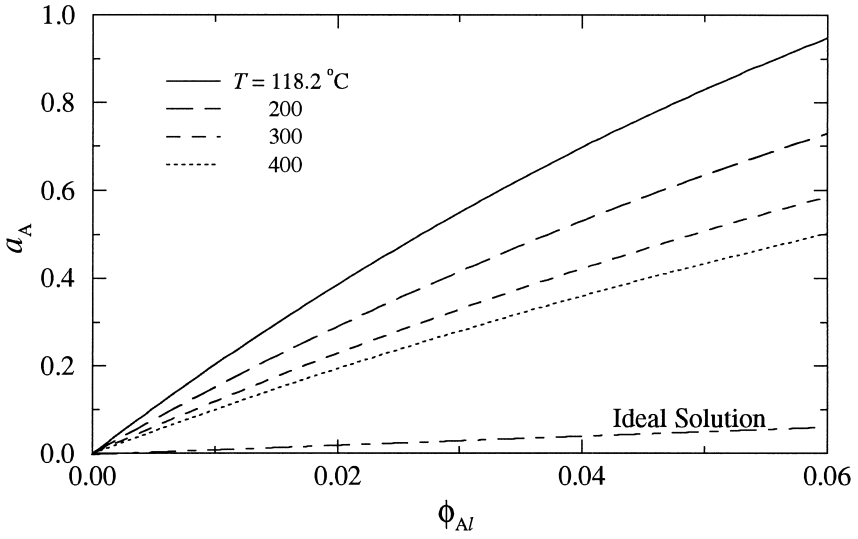

Fig. 5. Activity coefficient of acetic acid in the polymer solution, a_A, as a function of the volume fraction of acetic acid, for three temperatures. The behavior of an ideal solution (Raoult's law) is also shown.

4.1.3. Activity parameters

The conservation equations, Eqs. (5) and (6), are solved, with the appropriate kinetics and diffusion coefficients, and the polymer solubility parameter is chosen to match the measured and predicted bloating temperatures, for each heating rate and specimen thickness. The saturation pressure of acetic acid has been obtained from the curve fit of the saturation pressure data presented by Aguilo et al. [18] (for the temperature range $0°C \leq T \leq 280°C$) using an Antoine-type equation, obtaining

$$\ln p_o = 22.9622 - \frac{4235.88}{T - 21.448}$$

where p_o (Pa) is the saturation pressure at T (K).

The reported solubility parameter for acetic acid is $\delta_A = 21.3$ MPa$^{1/2}$ (obtained from the enthalpy of vaporization) [10]. Fig. 4(c) shows the values obtained for the polymer solubility parameter δ_{PA} as a function of specimen thickness and heating rate. The average value for δ_{PA} is 11.4 MPa$^{1/2}$. The specimens with smaller thicknesses give solubility parameters very close to the average and the scatter increases for the thicker samples. This may be attributed either to the uncertainties in the diffusion coefficient (as diffusion becomes more important for the thick samples) or to a stronger concentration dependence of the solubility parameter when the concentration of acetic acid increases. Grulke [10] reports values for the solubility parameter of EVA varying between 0 and 17, for strong solvent hydrogen bonding to poor solvent hydrogen bonding. Acetic acid is considered a moderate hydrogen bonding solvent [10]. Thus, $\delta_{PA} = 11.4$ MPa$^{1/2}$ is adopted here.

Fig. 5 presents the activity of acetic acid in the polymer as a function of the volume fraction of acetic acid for various temperatures. The curves show a large positive deviation from Raoult's law (ideal solution) and a strong dependence on temperature. The fraction of acetic acid present in the EVA ($Y_{A-PA} = 0.125$) corresponds to $\phi_{A,l} = 0.115$. The pre-charge shown in Fig. 4(a) corresponds to $\phi_{A,l} = 0.00613$. In this range of volume fractions, we observe an almost Henrian behavior for the activity. This is expected from the limit of the Flory–Huggins equation for small solvent concentrations. The polymer solubility parameter (and the corresponding activity curves) can be considered as an approximation for these relatively small values of volume fraction. Extrapolations beyond these values are not recommended.

4.2. Effect of sample size and heating rate on bloating temperature

The model is used to predict the binder removal and the acetic acid gas pressure histories with respect to temperature, for different heating rates. Fig. 6(a) shows the mass fraction of the binder remaining, $1-\eta$, and the pressure of the acetic acid p_A, for a 4 mm specimen with a pre-charge of $\langle \rho_{A,l} \rangle_i / \langle \rho \rangle = 0.0015$ under different constant heating rates dT/dt. For $dT/dt = 0.1°C$ min^{-1}, the pressure initially increases due to the pre-charge, then decreases when the pre-charge is removed, and then increases again due to the generation of acetic acid from the thermal degradation of

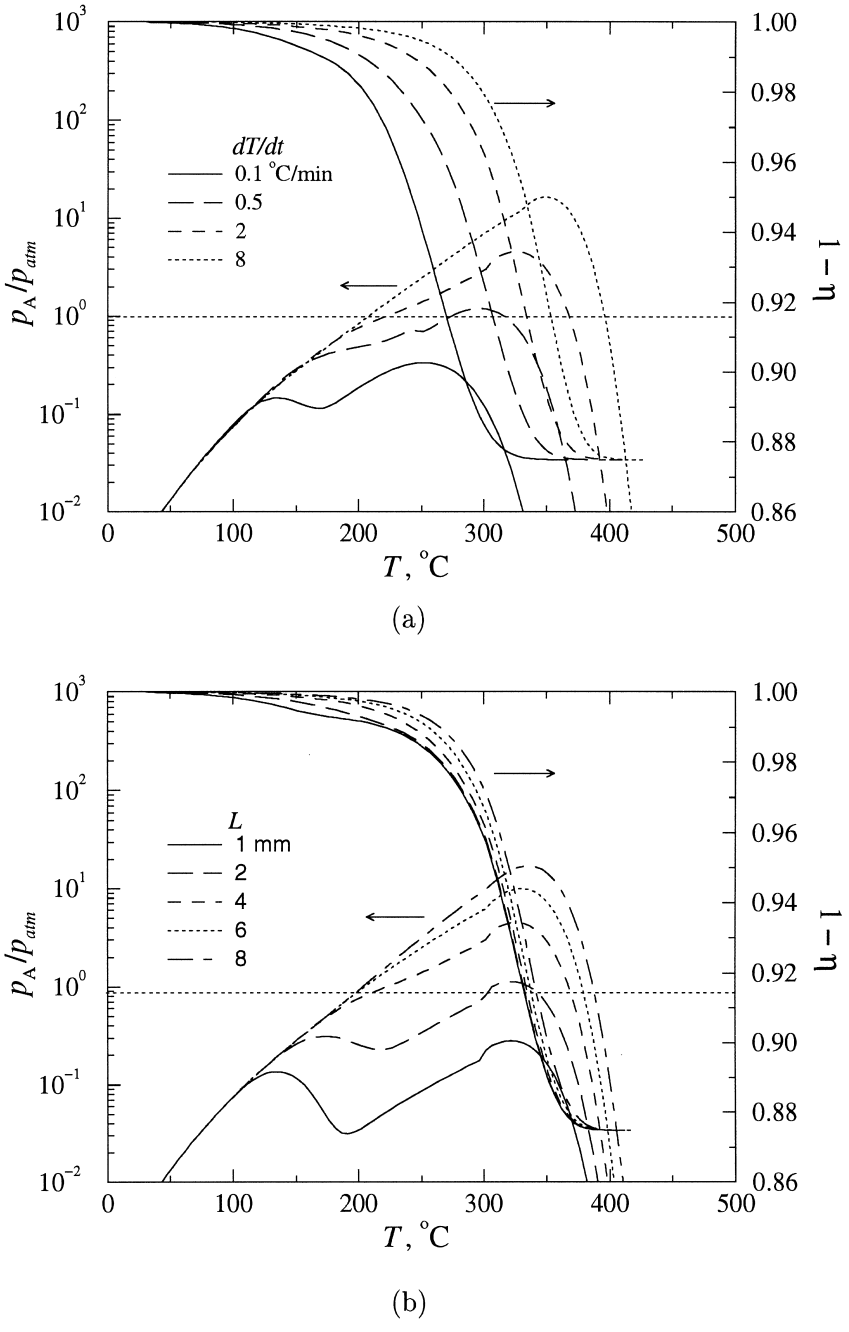

Fig. 6. (a) Evolution of the binder removal $(1-\eta)$ and the pressure of acetic acid p_A for four different heating rates (for a 4 mm thick specimen). (b) Evolution of the binder removal $(1-\eta)$ and the pressure of acetic acid p_A for four different specimen thicknesses and for a heating rate of $2°C/min^{-1}$.

the EVA. For this low heating rate, there is no bloating (for a 1 atm ambient pressure). As the heating rate is increased to $0.5°C\ min^{-1}$, bloating occurs in the second peak in the pressure curve, due to the generation of acetic acid (and not the pre-charge). A further increase in the heating rate moves the bloating to the first peak and the corresponding bloating temperature suffers a sudden drop. This bloating is caused by the pre-charge. Different amounts of the pre-charge tend to change only the height of the first peak, leaving the

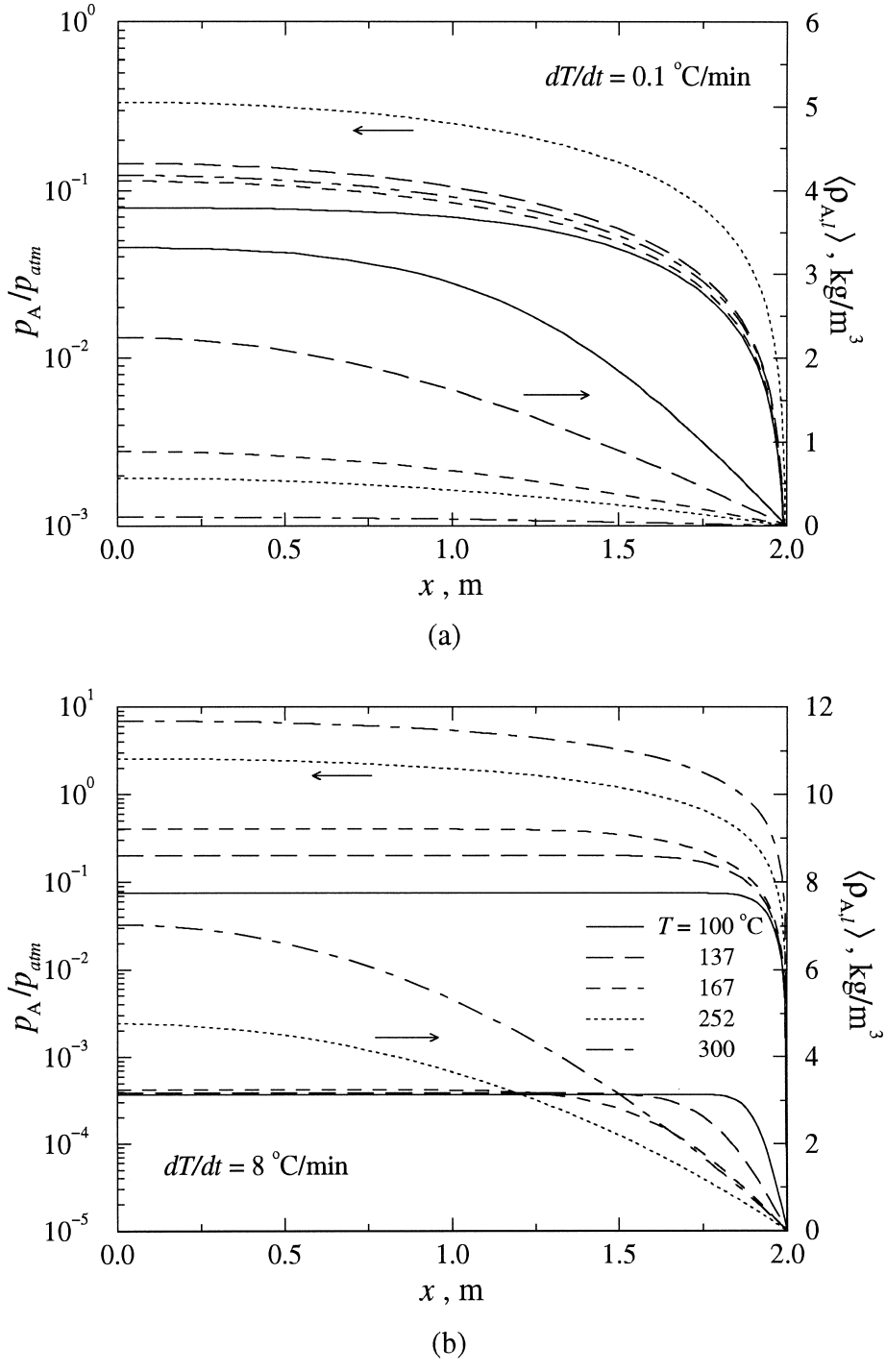

Fig. 7. Variation of the local volume-averaged mass concentration of acetic acid $\langle \rho_{A,l} \rangle$ and acetic acid pressure p_A, at the center-plane of the specimen, with respect to the x-axis. The results are for the heating rates of (a) $dT/dt = 0.1°C\ min^{-1}$ and (b) $dT/dt = 8°C\ min^{-1}$, and for five different temperatures [the legend for (b) applies also to (a)].

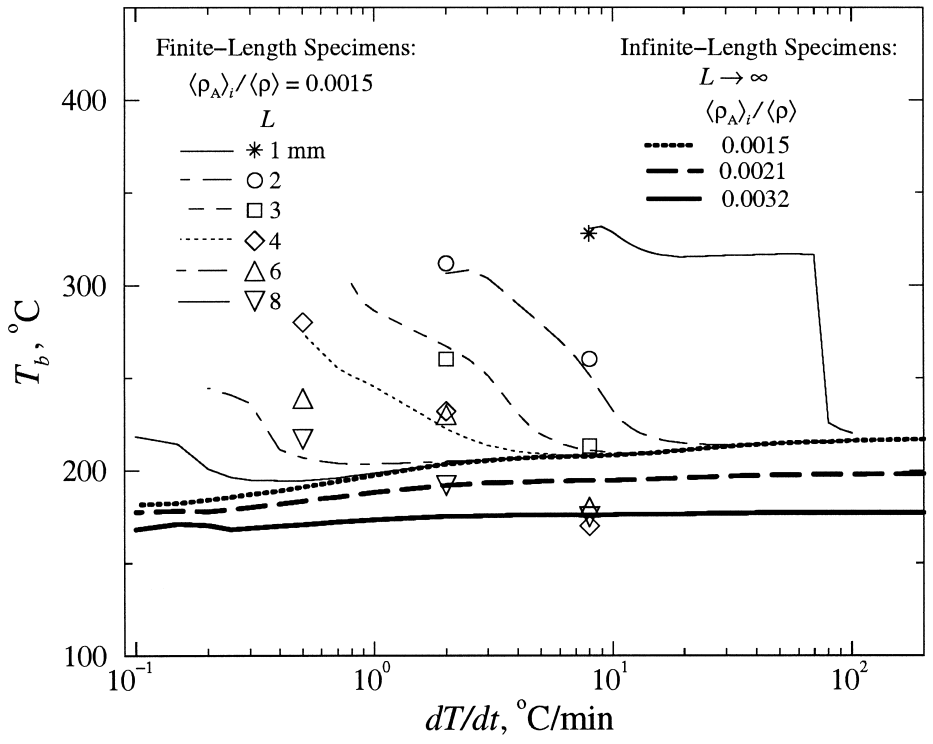

Fig. 8. Variation of the measured and predicted bloating temperature T_b with respect to the heating rate dT/dt, for six different sample thicknesses using a pre-charge of $\langle\rho_{A,l}\rangle_i/\langle\rho\rangle = 0.0015$. Also shown are the predictions for an infinitely thick specimen $L \to \infty$, for three values of the pre-charge.

second peak unaltered. Fig. 6(b) shows the predictions for different specimen thicknesses for $dT/dt = 2°C\ min^{-1}$. The trends are similar to the ones in Fig. 6(a). The binder removal curve for the 1 mm thick specimen shows a sharp distinction between the removal during the pre-charge controlled regime and the generation and removal of acetic acid period (around 200°C). For the thicker specimens there is an overlap of these two periods due to a delay in the removal of the pre-charge.

Fig. 7 presents the distributions of the local volume-averaged concentration of acetic acid $\langle\rho_{A,l}\rangle$ and gas pressure p_A with respect to x for a 4 mm thick specimen under two different constant heating-rates [the legend on Fig. 7(b) also applies to Fig. 7(a)]. For $dT/dt = 0.1°C\ min^{-1}$ [Fig. 7(a)], although $\langle\rho_{A,l}\rangle$ decreases monotonically, p_A has a maximum for $T = 252°C$ and then decreases (this can also be seen in Fig. 6). For $dT/dt = 8°C\ min^{-1}$ [Fig. 7(b)] the depth of penetration of the diffusion front is smaller. The generation of acetic acid is shown to peak at T between 170 and 250°C. For the temperatures plotted, p_A increases monotonically, causing bloating at $T = 205°C$ (from Fig. 6). This bloating occurs in a period where generation is just starting and it occurs primarily due to the pre-charge.

The bloating temperatures are plotted in Fig. 8 as a function of the heating rate for different sample sizes (the thin lines are the predictions and the symbols are the experiments). To the left of the final point in the curves (i.e., small heating rates), no bloating occurs. The uncertainty in the experimental results, obtained from repeating the experiments (at least two repetitions for each sample size), is estimated to be ±10°C. This is the uncertainty for the bloating temperatures that occurred due to the pre-charge. Small variations on the amount of pre-charge due to variations on the conditions during the specimen's manufacturing result in larger variations on the bloating temperature. The bloating temperatures that occur after the removal of the pre-charge have smaller uncertainties associated to them. We observe that the model closely predicts the bloating temperature for the thinner specimens and the difference increases for the thicker specimens. This lack of agreement for the thicker specimens is, probably, mostly due to the uncertainties in the parameters for the diffusion coefficient. Note also that a different amount of pre-charge for the thicker specimens, when

compared to the thinner specimens, could explain the differences observed. This will be discussed below. Another possible source of error is the experimental time constant for the heating and cooling of the specimens, discussed in the next section.

Fig. 8 shows that for sufficiently high heating rates, all curves collapse into a single curve (for a given amount of pre-charge). This asymptote for high heating rates depends only on the amount of pre-charge (it is independent of sample size), because for high heating rates there is not enough time to diffuse away the pre-charge before the pressure at the center of the specimen reaches the threshold value [Fig. 7(b)]. For a finite-size specimen, when the heating rate decreases, diffusion is able to eliminate the pre-charge and bloating occurs at higher temperatures [related to the second peak in the pressure curve in Fig 6(a)]. However, for infinite-size specimens, the bloating temperature increases with heating rate. The bloating temperature for infinite-length specimens can be obtained from thermodynamic considerations. Under the assumption of dilute solution, using the Clausius–Clapeyron equation to model the saturation vapor–pressure curve, and assuming the zeroth-order degradation kinetics only, the equation for the bloating line (bloating temperature T_b as a function of the heating rate dT/dt) for the limit of infinite sample size can be given in closed form as [19]

$$\frac{-R_g T_b^2 \gamma^o_{A,S}}{\Delta h_{A,lv} - \Delta u_{A,PA,lv}} \frac{A_{o,\phi} \exp\left(-\dfrac{\Delta E_a}{R_g T_b}\right)}{dT/dt} + \exp\left(\frac{\Delta h_{A,lv} - \Delta u_{A,PA,lv}}{R_g T_b} - \frac{\Delta h_{A,lv}}{R_g T_{sat}(p_t)}\right) = \phi_{A,l,i}\gamma^o_{A,S} \tag{29}$$

where $\phi_{A,l,i}$ is the initial volume fraction of acetic acid due to the pre-charge, dT/dt is the heating rate (in $^\circ C\ s^{-1}$), $\Delta h_{A,lv}$ is the heat of vaporization of acetic acid, and $A_{o,\phi}$, $\Delta u_{A,PA,lv}$, and $\gamma^o_{A,S}$ are given by

$$A_{o,\phi} = \frac{\rho_{PA,l}}{\rho_{A,l}} A_{o,\eta}, \quad \Delta u_{A,PA,lv} = V_A(\delta_{PA} - \delta_A)^2, \quad \gamma^o_{A,S} = \exp(1 + \chi_S). \tag{30}$$

The first term in Eq. (29) is related to the kinetics of the thermal degradation while the second term is related to the phase equilibrium. Note that the chemical (pseudo-) equilibrium constant $k_\phi = A_{o,\phi} \exp(-\Delta E_a/R_g T_b)$ is itself a function of the heating rate dT/dt. The first-order reaction period is not necessary here, but it can be easily accounted for, since in the dilute solution limit the expression for the first-order kinetics becomes zeroth-order. To calculate the asymptotes, the Clausius–Clapeyron equation was curve-fitted to the saturation pressure data obtaining

$$\ln\left(\frac{p_o}{p_{atm}}\right) = -4644.30\left(\frac{1}{T_{sat}} - \frac{1}{391.35}\right) \tag{31}$$

where T_{sat} is in K.

From this curve fitting, we obtain $\Delta h_{A,lv} = 3.86 \times 10^7$ J kmol^{-1} (in contrast to the tabulated value of $\Delta h_{A,lv} = 2.37 \times 10^7$ J kmol^{-1} found in the literature for $T = 391.35$ K).

Eq. (29) can be solved for T_b for different values of dT/dt and $\phi_{A,l,i}$. The thick lines on Fig. 8 are the results obtained from Eq. (29) for three different values of the pre-charge. The bloating temperature increases with heating rate because, although the chemical kinetic constant k_ϕ increases with heating rate, the increase in dT/dt itself overcomes that effect causing the first term in Eq. (29) to decrease. Physically, an increase in the heating rate causes a decrease in the time available for degradation and therefore smaller amounts of acetic-acid are formed. In the limit of infinite heating rate, no acetic acid is formed and bloating occurs due to the pre-charge only. It is important to notice that the kinetics was measured for heating rates up to $dT/dt = 16^\circ C\ min^{-1}$ and extrapolations beyond this limit are not warranted. Note also that the curve corresponding to $\langle \rho_{A,l} \rangle_i / \langle \rho \rangle = 0.0032$ gives bloating temperatures equal to the experimental results for the 8 mm thick specimens, showing the strong effect that variations in the pre-charge have in the bloating temperature.

In the limit of infinite heating rate, Eq. (29) can be further simplified to

$$\frac{T_b}{T_{sat}(p_t)} = \frac{(\Delta h_{A,lv} - \Delta u_{A,PA,lv})}{R_g T_{sat}(p_t)\ \ln(\phi_{A,l,i}\gamma^o_{A,S}) + \Delta h_{A,lv}}. \tag{32}$$

which is the equation for the equilibrium temperature in which $p_A = p_t$ for a given amount of pre-charge.

The agreement between Eqs. (29) and (32) and the numerical results is very good (there is less than 2% difference).

At the bloating temperature, as in the bloating maps (Fig. 8 and [8]), the specimen integrity is already compromised. For the development of an optimum schedule, a holding diagram needs to be developed and this is described below.

4.3. Heating schedule for defect-free specimen

A two-period debinding schedule is developed by finding a single temperature to which the specimen temperature can be raised, using a constant heating rate, and then maintained until the completion of the thermal degradation (of acetic acid) without the occur-

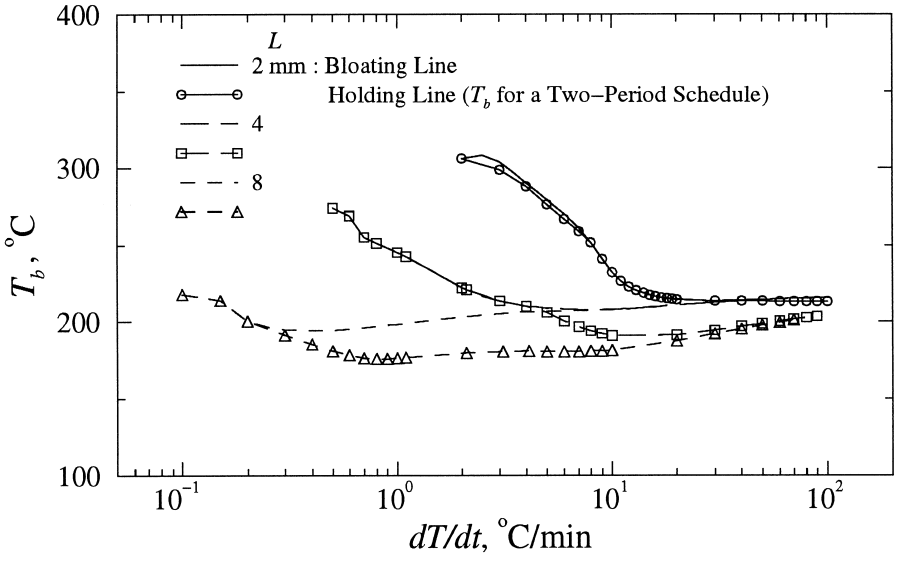

Fig. 9. Comparison of the predicted holding lines (lines of safe temperature for a two-period debinding schedule with respect to the heating rate) with the predicted bloating lines.

rence of bloating. The loci of these temperatures T_h in the bloating temperature T_b vs. heating rate dT/dt diagram will be referred to as the holding line. The specimen can be maintained indefinitely at $T = T_h$ without bloating. For $T > T_h$ the specimen is already compromised and only rapid cooling may prevent the bloating.

Fig. 9 shows the holding and bloating lines for three specimen thicknesses. For small heating rates, the bloating lines and the holding lines coincide. This occurs because at high temperatures the diffusion is able to remove the acetic acid generated. Once the threshold of bloating is avoided, the temperature can be kept constant and the pressure of acetic acid drops immediately. For larger heating rates the holding line is at smaller temperatures compared to the bloating line. Therefore, when the temperature is kept constant at the holding temperature, the pressure of acetic acid continues to increase and then drops only at higher temperatures, when diffusion becomes significant. For very large heating rates, $dT/dt \to \infty$, the bloating and holding lines coincide again (i.e., bloating occurs at the saturation curve). The difference between the bloating and the holding lines could also explain the deviations observed in Fig. 8 for the bloating temperature in the case of thicker specimens. The cooling of the thicker specimens, upon reaching the test temperature, is slower than the thinner specimens. Then, the bloating temperature detected is influenced by the cooling time (which behaves similar to a hold).

From Fig. 9, it seems that the strategy to develop an optimum schedule is to use a sequence of periods each of them having the maximum heating rate dT/dt for that period, such that when the temperature is kept constant at the end of the period, bloating never occurs. This is similar to determining a series of holding lines, at prescribed time intervals, each of them using the maximum (and safe) heating rate possible. This leads to a substantial reduction in the total thermal debinding time t_A, as is shown next.

4.4. Development of an optimum schedule

This optimum schedule consists of minimizing the total time

$$t_A = \sum_{j=1}^{N} \Delta t_j = \sum_{j=1}^{N} \frac{\Delta T_j}{\left(\frac{dT}{dt}\right)_j}. \tag{33}$$

Minimizing the total time, implies maximizing the heating rate $(dT/dt)_j$ for each period. This maximization is constrained by

$$\frac{p_A(x=0)}{p_t} \le 1 \tag{34}$$

where $p_A(x=0)$ is the pressure of acetic acid at the centerplane of the specimen.

This optimization procedure has been implemented as a root-finding scheme. For each period, a search method is used to find the heating rate $(dT/dt)_j$ that

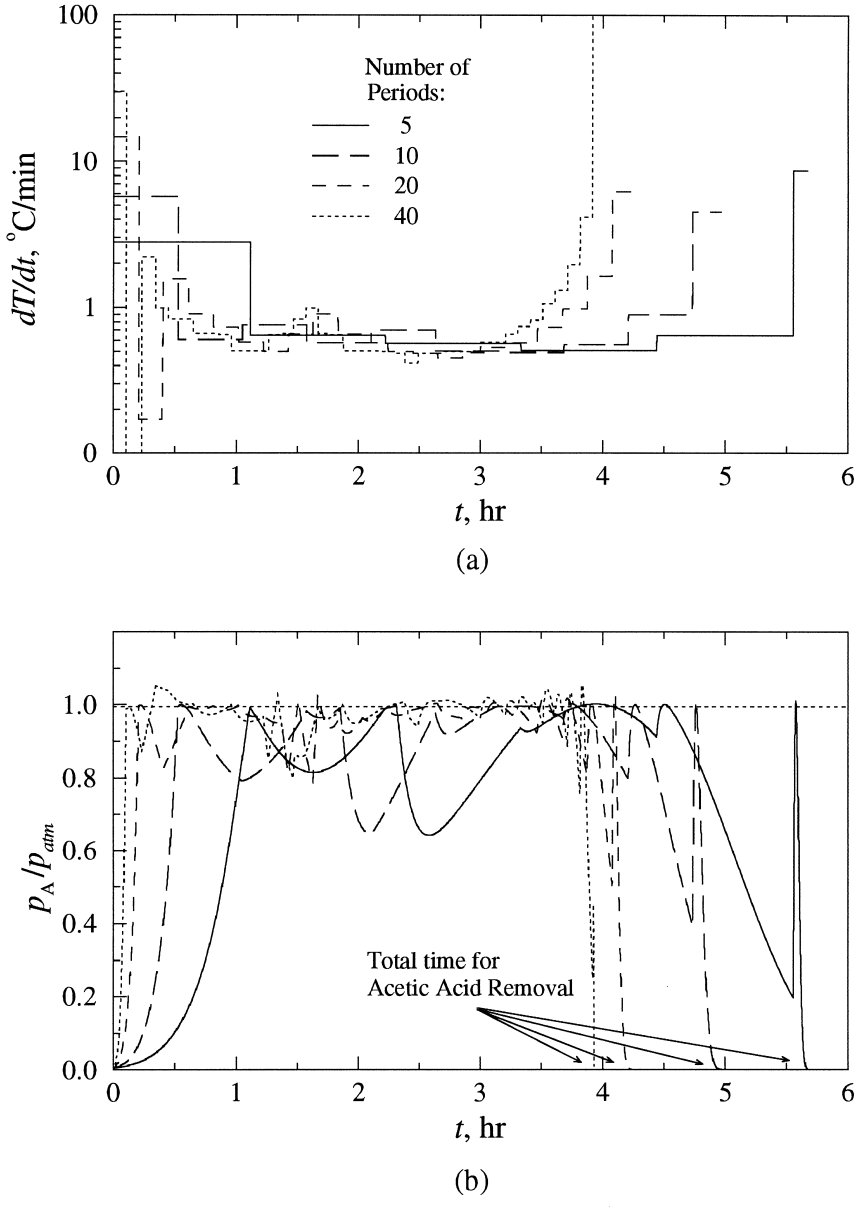

Fig. 10. (a) The optimum variation of the heating rate dT/dt, and (b) the pressure of acetic acid p_A at the centerplane, with respect to the elapsed time. The results are for the optimum schedules with 5, 10, 20, and 40 equal time periods and for a 4 mm thick specimen.

gives $p_A(x=0)/p_t-1=0$ for any time within the current Δt_j or beyond. This process is then repeated for the next time intervals, $j+1$, until complete removal of the acetic acid is achieved.

Fig. 10(a) presents the optimum schedules for a 4 mm specimen using Δt of 1 h, 30, 10, and 5 min (N equal to 5, 10, 20, and 40 periods). We note that as Δt decreases, the heating rate curve for the optimum schedule approaches a continuous variation and the thermal debinding time approaches a minimum. For $\Delta t=5$ min the total time is 3.9 h. This represents a reduction of 66% in the debinding time when compared to 12.1 h obtained for a single period. The heating rate curve for $\Delta t=5$ min presents initially a high heating rate. This is used to raise the temperature of the specimen until it reaches the holding line shown in Fig. 9.

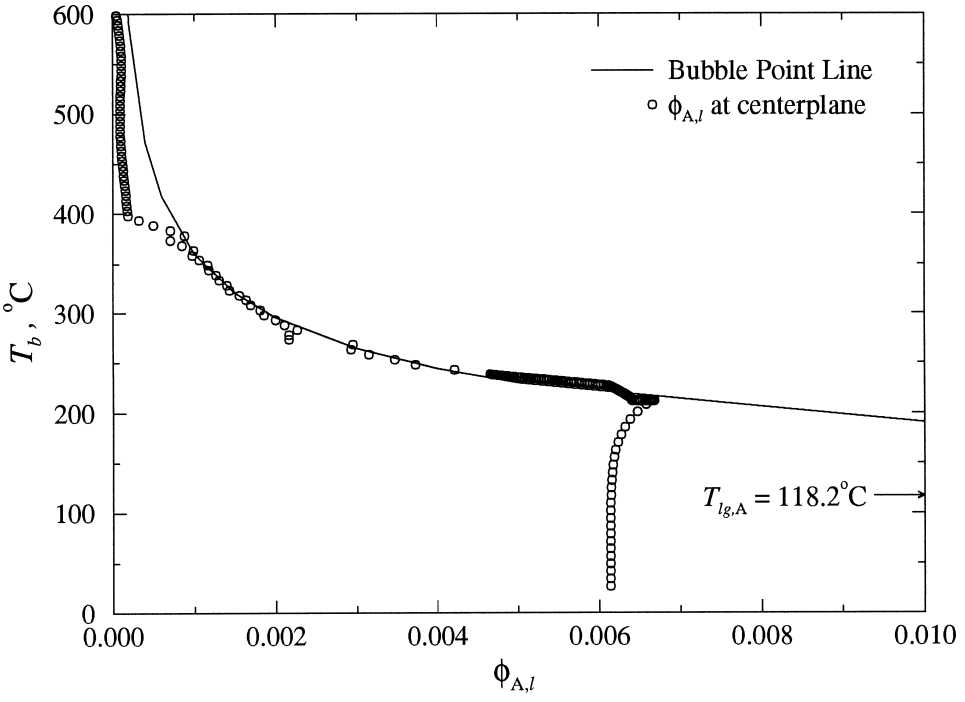

Fig. 11. Bubble-point line for the acetic acid-polymer solution at $p=1$ atm and $\phi_{A,l}$ at the center plane of the specimen during debinding following the optimum schedule for a 4 mm thick specimen.

For the limit when $\Delta t \to 0$ this initial heating rate is infinite. The next heating period occurs with an almost zero heating rate. This is necessary for the removal of the pre-charge without bloating. After removing part of the pre-charge, the heating rate is slightly increased and the removal of the generated acetic acid occurs. When the generation decreases as t_A is approached, the heating rate can be raised again to complete the acetic acid removal. Fig. 10(b) presents the variation of p_A with respect to time for the schedules in Fig. 10(a). In the initial periods, the pressure reaches its maximum at the end of each period. As time increases, the maximum in the pressure occurs within the following period. This justifies the approach used for the optimization and is in accordance with the results showed in Fig. 6.

Another way of visualizing the optimum schedule is possible when it is plotted in the phase diagram for the mixture. Fig. 11 shows the bubble-point line (or boiling line) for the acetic acid/liquid polymer mixture at $p=1$ atm. The circles are the temperature and volume fraction of acetic acid at the centerline of the specimen during the optimum schedule for a 4 mm thick specimen. Note that for an optimum schedule, the temperature is raised to the saturation temperature (for the given amount of pre-charge) as fast as possible and then it follows the bubble-point line, until the amount of acetic acid produced is much smaller than the diffusion rate. Therefore, for the optimum schedule the heating rate is modulated such that for a given temperature $\phi_{a,l}(x=0)=(\phi_{a,l})_{sat}$.

Fig. 12(a) shows the evolution of the temperature and the remaining binder mass for the optimum schedules. The small plateau observed in the temperature curves is related to the removal of the pre-charge, and becomes more noticeable as the number of periods is increased. The long period with an almost constant heating rate is related to the generation and removal of acetic acid. Fig. 12(b) shows the evolution of the mass flux at the surface (mass loss), the total generation rate, and the ratio of the two. Neither the mass loss nor the mass generated are constant during the acetic acid removal. Their ratio tends to one over all the generation and removal periods. During the pre-charge removal, the ratio deviates from unity, since the generation is practically zero.

Fig. 13(a) presents a regime diagram where the pre-charge dominated regime and the generation-dominated regime are shown. Although the generation-dominated regime is the most time consuming, the pre-charge dominated regime is the most critical, requiring smaller heating rates.

Fig. 13(b) presents the variation of the total acetic acid removal time t_A with respect to the number of

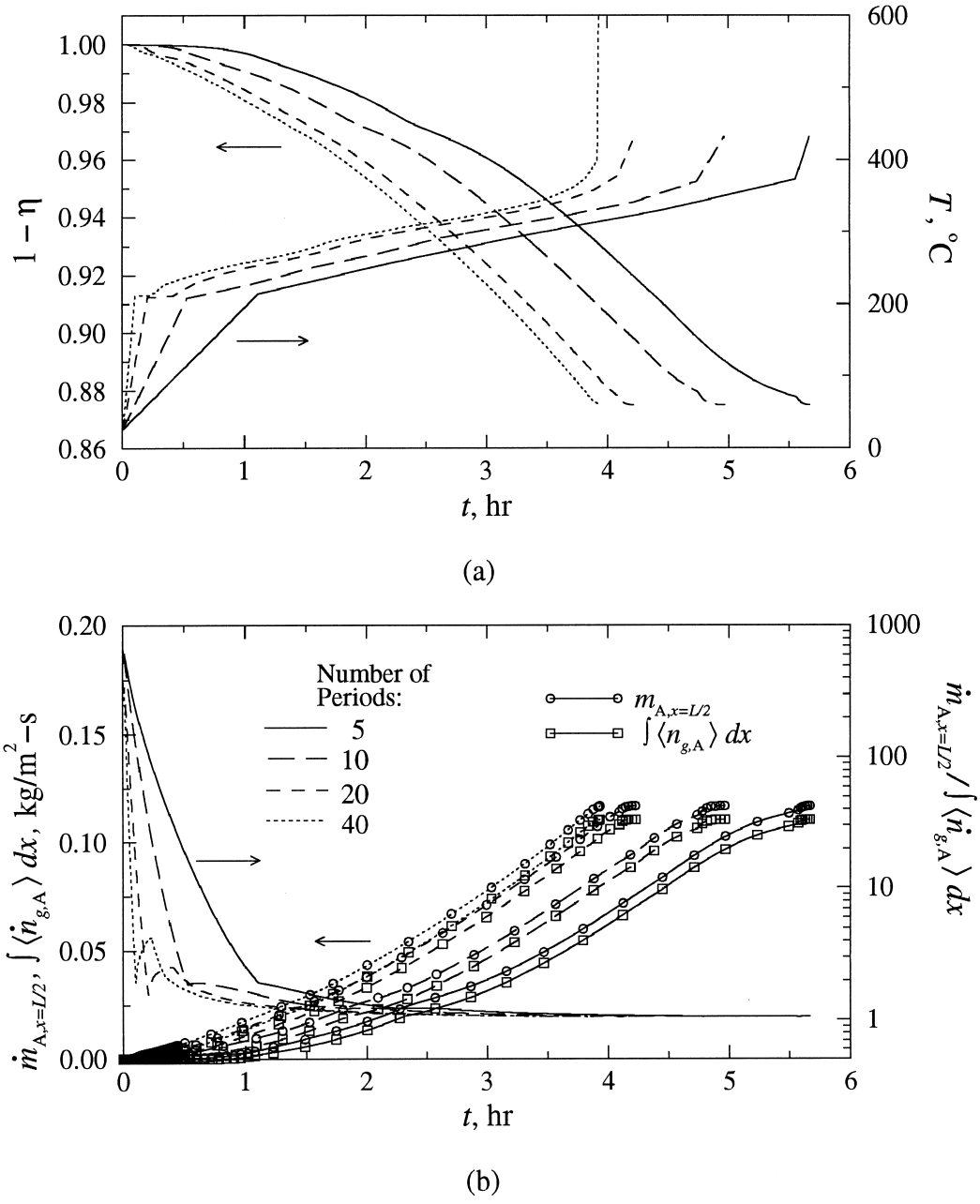

Fig. 12. (a) Variation of the mass fraction of the polymer remaining, $1-\eta$, and temperature T, and (b) the mass flux of acetic acid at the specimen surface (mass loss per unit time and unit area) and the total mass of acetic acid generated, as a function of time for the optimum schedules. The results are for 5, 10, 20, and 40 equal time periods, for a 4 mm thick specimen.

periods N. We note a significant reduction in t_A when the number of periods is increases from 2–4, and then a relatively smaller gain for further increases in N. For all the three specimens, there is an approximate 70% reduction in debinding time when comparing the single-period to the multi-period schedule ($N=40$). For practical purposes, the obtained optimum schedule may be approximated by a finite number of periods. The optimum schedule in Fig. 10(a), could be conveniently approximated by a five-period schedule.

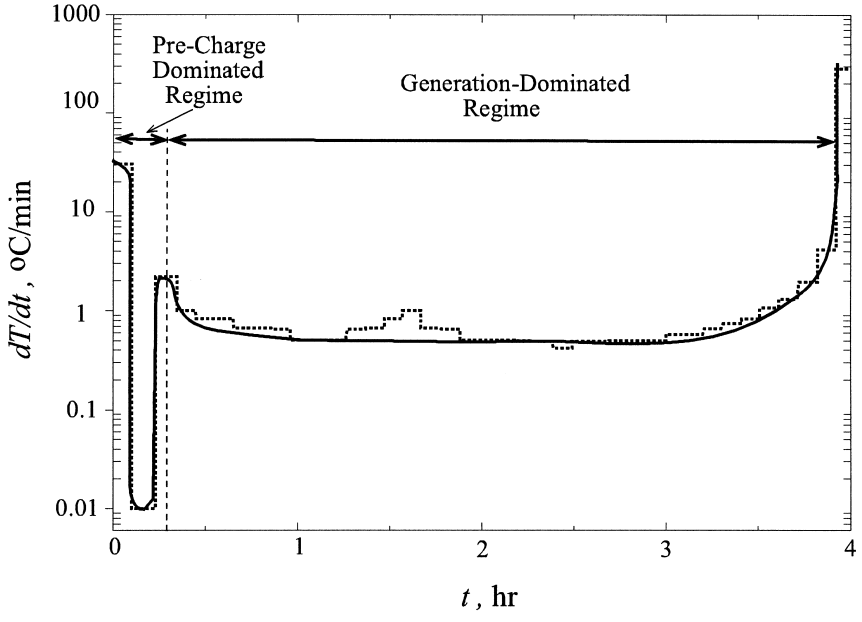

(a)

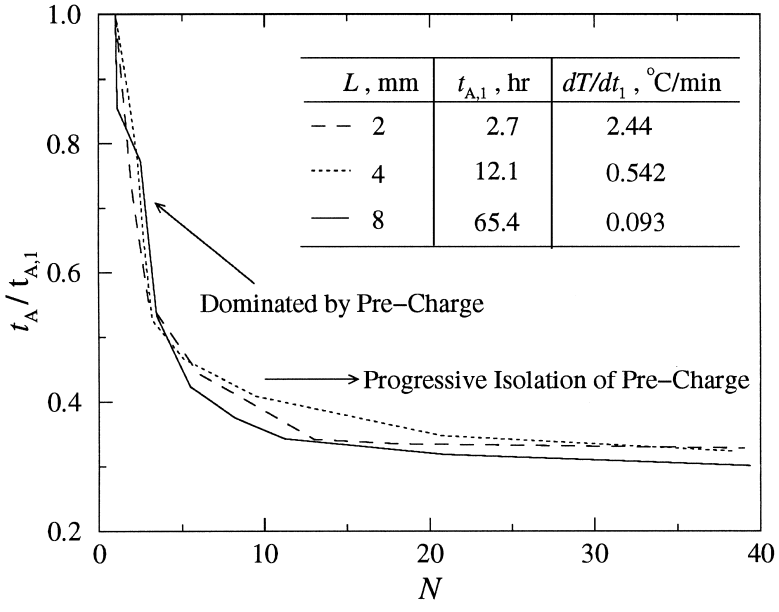

(b)

Fig. 13. (a) Regime diagram for the binder removal showing the pre-charge dominated regime and the generation-dominated regime. (b) Variation of the total time for the removal of acetic acid t_A as a function of the total number of periods N.

5. Conclusions

The gas pressure evolution in the early stages of the thermal degradation is modeled using the experimental degradation kinetics, a thermodynamic model for the gas–liquid equilibrium, a model for the diffusion coefficient, and the species conservation principle.

The comparison of the predicted and measured bloating temperatures is considered acceptable for the thin specimens and deviates for the thick specimens. This is mostly attributed to the uncertainties in the diffusion coefficient. The deviation may also be the result of experimental uncertainties related to the small variations in the pre-charge and related to the relatively slow cooling process suffered by the thicker specimens.

The development of the optimum schedule is based on the constrain that for a defect-free thermal debinding, the partial pressure of acetic acid should be smaller than (or equal to) the threshold pressure during the entire binder removal period. Under this constraint, the maximum heating rate for each of a given number of heating periods of equal time increment is found. A single-period schedule is dominated by the effect of the pre-charge, which increases in importance for thicker specimens. Then, a low heating-rate is required to overcome the elimination of the pre-charge period without bubbling. As the number of heating-rate periods increase, the effect of the pre-charge is progressively isolated, thus decreasing the amount of time necessary for the acetic acid removal. For an infinite number of periods, the heating rate history becomes continuous, thus giving the minimum time for a defect-free thermal debinding. Two regimes are identified. In the generation-dominated regime, the threshold of bloating is determined from a balance between the generation and diffusion rates of acetic acid. For the pre-charge dominated regime, the bloating is determined from a balance between the storage and diffusion rates.

It is shown that the use of the optimum schedule, when compared to a single-period schedule, reduces the total time for the removal of acetic acid. For example, for a 4 mm thick specimen, this represents a 68% time saving (from 12.1 to 3.9 h), and for a 8 mm thick specimen, this represents a 70% time saving (from 65.4 to 19.7 h). This optimum schedule can then be approximated by a smaller number of periods, for example, five periods.

The major limitation of the model is the simple Arrhenius relation used for the diffusion coefficient. This relation includes a set of parameters determined empirically. Here the parameters for the diffusion coefficient were obtained using a single heating rate. For experimental verification of the optimum schedule, these parameters should be obtained and averaged using various heating rates. This requires further experiments and is left for future reportings.

The conclusions obtained here can also be applied to the case in which the polymer blend has a low boiling-point species as a component (e.g., [6,7]). This species would have the role of the pre-charge examined here.

Acknowledgements

The authors acknowledge the financial support of the Conselho Nacional de Desenvolvimento Científico e Tecnológico—CNPq, Brazil, and the US National Science Foundation. Drs Richard Fox and Tim Fawcett of Dow Chemical Company and Professor Randall German have encouraged this study and for that we are very thankful. Brian D'Amico's assistance with the experiments is greatly appreciated.

References

[1] K. Hrdina Phenomena during thermal removal of binders. PhD thesis, Department of Materials Science and Engineering, The University of Michigan, Ann Arbor, MI, 1997.

[2] J.R.G. Evans, M.J. Edirisinghe, J.K. Wright, J. Crank, On the removal of organic vehicle from moulded ceramic bodies. Theoretical models for binder burnout, Proc. R Soc. London A 432 (1991) 321–340.

[3] P. Calvert, M. Cima, J. Am. Ceram. Soc. 73 (1990) 575–579.

[4] S.A. Matar, M.J. Edirisinghe, J.R.G. Evans, E.H. Twizell, The influence of monomer and polymer properties on the removal of organic vehicle from ceramic and metal moldings, J. Mater. Res. 10 (1995) 2060–2072.

[5] H.M. Shaw, M.J. Edirisinghe, Shrinkage and particle packing during removal of organic vehicle from ceramic injection mouldings, J. Eur. Ceram. Soc. 45 (1995) 109–116.

[6] M.R. Barone, J.C. Ulicny, Liquid-phase transport during removal of organic binders in injection-molded ceramics, J. Am. Ceram. Soc. 73 (1990) 3323–3333.

[7] G. Stangle, I.A. Aksay, Simultaneous momentum, heat, and mass transfer with chemical reaction in a disordered porous medium: application to binder removal from a ceramic green body, Chem. Engng Sci. 45 (1990) 1719–1731.

[8] I.E. Pinwill, M.J. Edirisinghe, M.J. Bevis, Development of temperature-heating rate diagrams for the pyrolitic removal of binder used for powder injection moulding, J. Mater. Science 27 (1992) 4381–4388.

[9] F.M. Barton, in: CRC Handbook of Solubility Parameters and Other Cohesion Parameters, 2nd ed., CRC Press, Boca Raton, FL, 1991, pp. 245–278 (Chapter 13).

[10] E.A. Grulke, Solubility parameter values, in: J. Brandrup, E.H. Immergut (Eds.), Polymer Handbook,

3rd ed., Wiley, New York, 1989, pp. 519–559 (Chapter VII).

[11] F. Gundert, B.A. Wolf, Polymer–solvent interaction parameters, in: J. Brandrup, E.H. Immergut (Eds.), Polymer Handbook, 3rd ed., Wiley, New York, 1989, pp. 173–185 (Chapter VII).

[12] K. Hrdina, J. Halloran, A.A.M. Oliveira, M. Kaviany, Chemistry of removal of ethylene vinyl acetate binders, Journal of Materials Science 33 (1998) 2795–2803.

[13] M. Kaviany, Principles of Heat Transfer in Porous Media, Springer-Verlag, New York, 1995.

[14] D.W. Van Krevelen, Properties of Polymers: Their Correlation with Chemical Structure; Their Numerical Estimation and Prediction from Additive Group Contributions, Elsevier, New York, 1990.

[15] A. Marcilla, M. Beltran, Kinetic study of the thermal decomposition of polystyrene and polyethylene-vinyl acetate graft copolymers by thermogravimetric analysis, Polymer Degradation and Stability 50 (1995) 117–124.

[16] I. Ray, S. Roy, T.K. Chaki, D. Khastgir, Studies on thermal degradation behavior of EVA/LDPE blend, Journal of Elastometers and Plastics 26 (1994) 168–182.

[17] M.D. Lechner, D.G. Steinmeier, Sedimentation coefficients, diffusion coefficients, partial specific volumes, frictional rates, and second virial coefficients of polymer and solutions, in: J. Brandrup, E.H. Immergut (Eds.), Polymer Handbook, 3rd ed., Wiley, New York, 1989, pp. 61–75 (Chapter VII).

[18] A. Aguiló, C.C. Hobbs, A.G. Zey, Acetic acid, in: W. Gerhartz (Ed.), Ullmann's Encyclopedia of Industrial Chemistry, 5th ed., VCH, Weinheim, Federal Republic of Germany, 1985.

[19] A.A.M. Oliveira Effect of particle- and specimen-level transport on product state in compacted-powder combustion synthesis and thermal debinding of polymers from molded powders. PhD thesis, Department of Mechanical Engineering and Applied Mechanics, The University of Michigan, Ann Arbor, MI, 1998.